

Proposal for midinfrared light-induced ferroelectricity in oxide paraelectrics

Alaska Subedi

*Centre de Physique Theorique, Ecole Polytechnique, CNRS,
Université Paris-Saclay, F-91128 Palaiseau, France and
Collège de France, 11 place Marcelin Berthelot, 75005 Paris, France*
(Dated: November 12, 2018)

I show that a nonequilibrium paraelectric to ferroelectric transition can be induced using mid-infrared pulses. This relies on a quartic $lQ_{1z}^2Q_{hx}^2$ coupling between the lowest (Q_{1z}) and highest (Q_{hx}) frequency infrared-active phonon modes of a paraelectric material. Density functional calculations show that the coupling constant l is negative, which causes a softening of the Q_{1z} mode when the Q_{hx} mode is externally pumped. A rectification along the Q_{1z} coordinate that stabilizes the nonequilibrium ferroelectric state occurs only above a critical threshold for the electric field of the pump pulse, demonstrating that this is a nonperturbative phenomenon. A first principles calculation of the coupling between light and the Q_{hx} mode shows that ferroelectricity can be induced in the representative case of strained KTaO_3 by a midinfrared pulse with a peak electric field of 17 MV cm^{-1} and duration of 2 ps. Furthermore, other odd-order nonlinear couplings make it possible to arbitrarily switch off the light-induced ferroelectric state, making this technique feasible for all-optic devices.

PACS numbers: 77.80.Fm, 78.20.Bh, 63.20.Ry, 78.47.J-

I. INTRODUCTION

Living organisms have used light to observe the properties of materials since the evolutionary development of complex eyes. However, ultrafast light-control of materials properties has only become feasible after the construction of high-powered lasers in the previous century, and this field has flourished because light-induced processes have the potential to lead to new devices and physical phenomena. Many examples of light-induced phase transitions using near-visible sources have been observed, including discontinuous volume changes in polymer gels,¹ quasiionic-to-quasineutral transition in organic molecular compounds,² low-spin to high-spin transition in metal organic frameworks,³ insulator-to-metal transition in perovskite manganites,⁴ and, remarkably, a transition to a hidden metastable state in $1T\text{-TaS}_2$.⁵ All of these examples involve transition to higher-temperature or metastable phases, and the quest to stabilize a phase with less symmetry or more order using light remains elusive.

More recently, intense midinfrared pulses have been used to directly control the dynamical degrees of freedom of the crystal lattice. Such mode-selective vibrational excitations have been used to induce insulator-to-metal transitions^{6,7} and melting of orbital⁸ and magnetic^{9,10} orders. Midinfrared excitations have so far not caused transitions to more-ordered phases, although light-induced superconductivity has been claimed in several cuprate compounds and K_3C_{60} .^{11–14} However, these claims rely on interpreting the two-dimensional response function $\Sigma(\omega, \tau)$ measured in the pump-probe experiments as the optical conductivity $\sigma(\omega)$ that is measured in time-domain spectroscopy. It is unclear whether such an interpretation is justified, especially at low frequencies, when the light-induced state is short-lived, as is the case in

these experiments.^{15,16} In any case, a light-induced transition to a lower-symmetry phase is not observed in any of these experiments. Nonetheless, midinfrared excitation should be an effective tool to drive materials to broken-symmetry phases because selective and coherent excitation of the low-energy structural degrees of freedom should cause minimal dissipation as heat.

The mechanism for mode-selective light-control of materials was proposed by Först *et al.*^{17,18} This involves exciting an infrared-active phonon mode Q_{IR} of a material using an intense light pulse which then causes the lattice to displace along a fully symmetric A_g Raman mode coordinate Q_{R} due to a nonlinear coupling $Q_{\text{R}}Q_{\text{IR}}^2$ between the two modes. A quantitative microscopic theory of this phenomenon was developed in Ref. 19, and calculations based on this theory in combination with a time-resolved x-ray diffraction experiment was used to resolve the midinfrared light-induced changes in the structure of $\text{YBa}_2\text{Cu}_3\text{O}_{6.5}$.²⁰ In addition to the historically discussed cubic order $Q_{\text{R}}Q_{\text{IR}_1}Q_{\text{IR}_2}$ coupling,^{21,22} Subedi *et al.* have shown that a sizeable quartic order $Q_{\text{R}}^2Q_{\text{IR}}^2$ coupling can occur and studied the dynamics due to such a coupling.¹⁹ They found that such a quartic coupling exhibits various distinct regimes of dynamics, including transient mode softening and dynamic stabilization in a rectified state. In contrast to the case of the cubic coupling, the displacement along the Q_{R} coordinate occurs only above a critical pump amplitude threshold for the quartic $Q_{\text{R}}^2Q_{\text{IR}}^2$ coupling. A more recent work has reproduced several aspects of the dynamics of this coupling.²³ Unlike the cubic $Q_{\text{R}}Q_{\text{IR}_1}Q_{\text{IR}_2}$ coupling,^{24,25} the $Q_{\text{R}}^2Q_{\text{IR}}^2$ coupling can cause a rectification along a symmetry breaking mode,¹⁹ but such a light-induced symmetry breaking of a crystal structure has so far not been observed.

It has recently been predicted that ferroelectric polarization can be switched using midinfrared pulses.²⁶ In this paper, I extend that work to the paraelectric phase

and show that ferroelectricity can also be induced in transition metal oxide paraelectrics. This relies on a quartic $lQ_{1z}^2Q_{hx}^2$ coupling and is a nonperturbative effect that occurs only above a critical pump amplitude. Here, Q_{hx} is a high-frequency infrared-active phonon mode that should be externally pumped and Q_{1z} is the lowest frequency infrared-active mode that is transverse to the pumped mode. I find that the sign of the coupling constant l is negative in several transition metal oxides, which causes the Q_{1z} mode to soften as the Q_{hx} mode is externally pumped. But other quartic order couplings $t_1Q_{1x}^3Q_{hx}$, $t_2Q_{1x}^2Q_{hx}^2$, and $t_3Q_{1x}Q_{hx}^3$ between Q_{hx} and the lowest frequency mode Q_{1x} that is longitudinal to the pumped mode are larger in magnitude. In the cubic materials, the couplings between Q_{1x} and Q_{hx} modes are such that the Q_{1z} mode may not develop a light-induced dynamical instability. However, I find that the couplings in the longitudinal direction can be effectively reduced by applying strain so that a light-induced ferroelectric state is stabilized by rectification along the Q_{1z} coordinate.

I illustrate this theory for the representative case of KTaO_3 to show that light-induced ferroelectricity can be generated in the strained version of this material when a pump pulse with an electric field of $\sim 17 \text{ MV cm}^{-1}$ and pulse duration of 2 ps is used. Interestingly, this value is noticeably smaller than what is expected for the critical pump amplitude due to a $Q_{1z}^2Q_{hx}^2$ coupling.¹⁹ I find that this reduction is due to the presence of substantial sixth order $Q_{1z}^4Q_{hx}^2$ and $Q_{1z}^2Q_{hx}^4$ couplings. Furthermore, I show that the light-induced rectification can be arbitrarily suppressed by pumping the highest frequency infrared-active mode Q_{hx} that is longitudinal to Q_{1x} with another weak pulse. Such a control is necessary for applications in devices. In addition to KTaO_3 , I find similar nonlinear couplings in SrTO_3 , and LaAlO_3 , and this technique could be generally applied to many transition metal oxide paraelectrics.

II. APPROACH

A. Computational details

The phonon frequencies and eigenvectors, nonlinear couplings between different normal mode coordinates, and the coupling between light and pumped infrared mode were all obtained from first principles using density functional calculations as implemented in the VASP software package. I used the projector augmented wave pseudopotentials provided with the package with the electronic configurations $3s^23p^64s^1$ (K), $5p^66s^25d^3$ (Ta), and $2s^22p^4$ (O, normal cut-off). A plane-wave cut-off of 550 eV for basis-set expansion, an $8 \times 8 \times 8$ k -point grid for Brillouin zone sampling, and the PBEsol version of the generalized gradient approximation was used.²⁷

The calculations were done using the relaxed lattice parameters for the cubic structure. For the strained structure, the c lattice parameter that minimized the total en-

ergy for the given strain was used. A very small energy convergence criteria of 10^{-8} eV was used in the calculations to ensure high numerical accuracy. After relaxing the lattice parameters, I calculated the phonon frequencies and eigenvectors using the frozen phonon method as implemented in the PHONOPY software package.^{28,29} After the normal mode coordinates were identified, total energy calculations were performed as a function of the Q_{1z} , Q_{1x} , and Q_{hx} coordinates for values ranging between -3 and $3 \text{ \AA}\sqrt{\text{amu}}$ with a step of $0.1 \text{ \AA}\sqrt{\text{amu}}$ to obtain the energy surfaces $V(Q_{1z}, Q_{1x}, Q_{hx})$. These were then fitted to polynomials given in Eq. A1 to obtain normal mode anharmonicities and nonlinear couplings between the three coordinates. For the materials that I explored, polynomials with anharmonicities up to twentieth order and nonlinearities up to eighth order were needed to ensure accurate fit to the calculated energy surfaces. Since the polynomial fits the calculated energy surfaces almost exactly, there are no approximations in the calculations of the nonlinear couplings, beyond that for the exchange-correlation functional.

The Born effective charges were calculated using density functional perturbation theory,³⁰ and a larger $16 \times 16 \times 16$ k -point grid was used in these calculations. The calculated Born effective charges and phonon mode eigenvectors were used to calculate the mode effective charge Z_m^* that determines the strength of the coupling of light to the pumped phonon mode from first principles.³¹ The coupled equations of motion for the three coordinates were numerically solved using the LSODE subroutine of the OCTAVE software package.³²

B. Identifying light-induced ferroelectricity

Phase transitions cannot occur at short timescales in nonequilibrium conditions, and any light-induced ferroelectricity will disappear once the external light source vanishes. Therefore, it is necessary to establish an unequivocal protocol for identifying light-induced ferroelectricity. Examining the intensity and phase of the second harmonic generation of the transmitted probe pulse is a convenient way to study ferroelectricity in pump-probe experiments,^{33,34} and it will be necessary to distinguish between light-induced ferroelectricity and a long-time-period excitation that both generate second harmonics if the probe pulse is shorter than the period of the low-frequency mode. For the purpose of this discussion, a light-induced ferroelectric state is deemed to have occurred both if the phase of the second harmonics does not change and the intensity of the second harmonics shows at least two peaks over the full width at half maximum (FWHM) duration of the pump pulse. Therefore, the pump pulse duration should in general be larger than the period of the equilibrium-condition lowest frequency mode to establish light-induced ferroelectricity. However, this is not a strict condition, and other well-defined criteria could also be specified. In particular, the lowest fre-

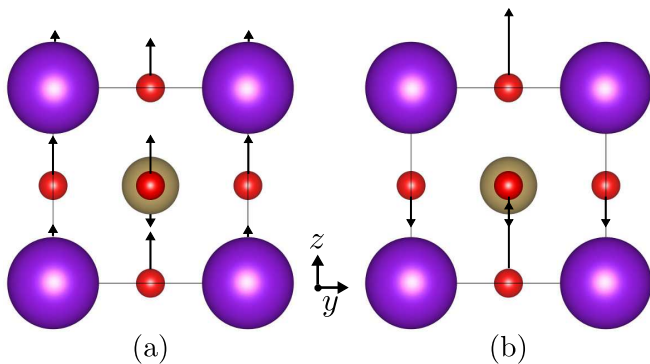


FIG. 1. (Color online) Displacement patterns of the (a) lowest frequency Q_{1z} and (b) highest frequency Q_{hz} modes of the cubic phase of KTaO_3 . The x and y components of these triply degenerate modes can be obtained by appropriate rotation. The big, medium, and small spheres denote K, Ta, and O, respectively.

quency oscillations could (and indeed does) occur with a larger frequency in the rectified state, and any method (such as time resolved x-ray diffraction) that can distinguish oscillations about a displaced position can establish light-induced ferroelectricity.

III. RESULTS AND DISCUSSIONS

A. Cubic KTaO_3

The paraelectric phase of several ABO_3 perovskite oxides occurs in the cubic structure. So it is natural to ask if ferroelectricity can be induced in these cubic paraelectrics by a midinfrared excitation of their infrared-active phonon modes. These materials have five atoms per unit cell, and they thus have four triply degenerate optical phonon modes at the zone center. Factor group analysis shows that three of these modes have the irreducible representation T_{1u} , and these are infrared active. The remaining one has the irreducible representation T_{2u} and is optically inactive. Ferroelectricity is generally ascribed to a dynamical instability of an infrared-active transverse optic phonon mode. Indeed, most ferroelectric materials show a characteristic softening of an infrared transverse optic mode as the transition temperature is approached.³⁵ Here I investigate if a similar softening and instability of the lowest frequency T_{1u} mode can be achieved by an intense laser-induced excitation of the highest frequency T_{1u} mode in the representative case of cubic KTaO_3 .

The calculated phonon frequencies of cubic KTaO_3 using the relaxed PBEsol lattice parameter of 3.99 Å are $\Omega_l = 85 \text{ cm}^{-1}$ and $\Omega_h = 533 \text{ cm}^{-1}$ for the lowest and highest frequency T_{1u} modes, respectively. These are in good agreement with previously calculated values.³⁶ They also agree well with the frequencies obtained from hyper-Raman scattering experiments at

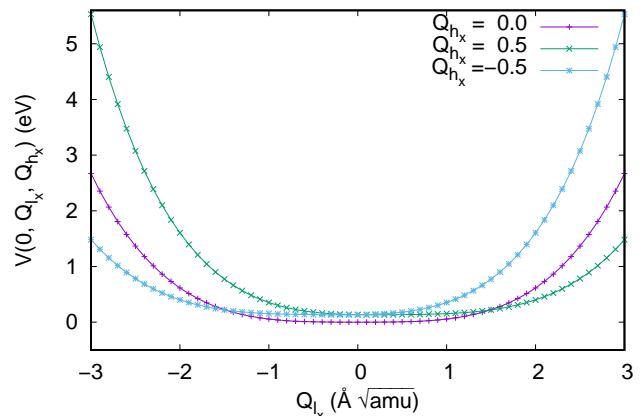


FIG. 2. (Color online) Total energy as a function of the longitudinal Q_{1x} coordinate for several values of the Q_{hx} coordinate for cubic KTaO_3 .

room temperature.³⁷ The atomic displacement patterns due to these two modes are shown in Fig. 1. Without loss of generality, I consider the case where the x component of the highest frequency T_{1u} mode Q_{hx} is pumped by an intense light source and study how such an excitation changes the dynamics of the lowest frequency T_{1u} mode along the longitudinal Q_{1x} and transverse Q_{1z} coordinates. I ignore the dynamics along the second transverse coordinate Q_{1y} as its dynamics will be qualitatively similar to that of the Q_{1z} coordinate.

1. Dynamics of the lowest frequency longitudinal component

Fig. 2 shows several total energy $V(Q_{1z}, Q_{1x}, Q_{hx})$ curves along the projection $Q_{1z} = 0$. The curves are not symmetric upon reflection at $Q_{1x} = 0$ and the $+Q_{hx}$ and $-Q_{hx}$ curves do not overlap. This indicates the presence of coupling terms that have odd orders of Q_{1x} and Q_{hx} . A polynomial fit of the energy surface shows that the coupling terms $t_1 Q_{1x}^3 Q_{hx}$, $t_2 Q_{1x}^2 Q_{hx}^2$ and $t_3 Q_{1x} Q_{hx}^3$ are all large relative to the harmonic term Ω_l^2 of the lowest frequency mode (see Table I). The presence of these couplings is consistent with the symmetry requirements. Since the equilibrium structure has inversion symmetry and we are considering two odd modes along the same direction, any term $Q_{1x}^m Q_{hx}^n$ is allowed as long as $m + n = \text{even}$. The next allowed order of coupling is $Q_{1x}^m Q_{hx}^n$ with $m + n = 6$. These are an order of magnitude smaller than the $m + n = 4$ terms (see Table II in the Appendix), but they are comparable in magnitude to the harmonic term Ω_l^2 .

The nonlinear couplings between the Q_{1x} and Q_{hx} modes impart a force equal to $-\partial V / \partial Q_{1x}$ along the Q_{1x} coordinate. This force is finite and large when the Q_{hx} mode is externally excited by an intense light source. The lowest order nonlinear terms of this force

TABLE I. The coefficients of the harmonic and nonlinear coupling terms of cubic and strained KTaO₃. The units of a $Q^m Q^n$ term are $\text{meV } \text{\AA}^{-(m+n)} \text{amu}^{\frac{-(m+n)}{2}}$. The sign of the coupling is relevant only when the coordinates come with even powers.

coefficient	order	cubic	strained
Ω_{1z}^2	Q_{1z}^2	27.06	1.39
Ω_{1x}^2	Q_{1x}^2	27.06	55.27
Ω_h^2	Q_{hx}^2	1043.77	1136.10
t_1	$Q_{1x}^3 Q_{hx}$	-118.35	97.38
t_2	$Q_{1x}^2 Q_{hx}^2$	215.00	208.76
t_3	$Q_{1x} Q_{hx}^3$	-175.58	195.22
l	$Q_{1z}^2 Q_{hx}^2$	-5.95	-5.81
m_1	$Q_{1z}^4 Q_{hx}^2$	-1.03	-1.00
m_2	$Q_{1z}^2 Q_{hx}^4$	-3.05	-4.12

are $-\partial V/\partial Q_{1x} = -3t_1 Q_{1x}^2 Q_{hx} - 2t_2 Q_{1x} Q_{hx}^2 - t_3 Q_{hx}^3$. The $-t_3 Q_{hx}^3$ term acts as a nonresonant oscillating force to the Q_{1x} mode. The effect of the $-3t_1 Q_{1x}^2 Q_{hx}$ term would average over the slow oscillation of the Q_{1x} mode relative to that of the Q_{hx} mode. The $-2t_2 Q_{1x} Q_{hx}^2$ term affects a time-dependent modulation of the frequency of the Q_{1x} mode, and it does not cancel over the slow oscillation of the Q_{1x} mode because Q_{hx}^2 has a nonzero time average.^{17,19} Unfortunately, the sign of t_2 is positive, so the frequency of the Q_{1x} mode increases as the Q_{hx} mode is pumped. A similar analysis of the next order $Q_{1x}^m Q_{hx}^n$ terms with $m+n=6$ also shows that the Q_{1x} mode does not soften due to the effects of nonlinear coupling terms.

2. Dynamics of the lowest frequency transverse component

What about the dynamics of the transverse component Q_{1z} of the lowest frequency mode? Fig. 3 shows several total energy $V(Q_{1z}, Q_{1x}, Q_{hx})$ curves along the projection $Q_{1x} = 0$. One immediately notices that the curves are symmetric upon reflection at $Q_{1z} = 0$ and that the $-Q_{hx}$ and Q_{hx} curves overlap, showing that only even powers of both Q_{1z} and Q_{hx} appear in the nonlinear coupling terms. This is again consistent with the symmetry requirements, which does not allow products with odd powers of mutually perpendicular components Q_{1z} and Q_{hx} . The coefficients of the lowest order nonlinear terms $lQ_{1z}^2 Q_{hx}^2$, $m_1 Q_{1z}^4 Q_{hx}^2$, and $m_2 Q_{1z}^2 Q_{hx}^4$ are given in Table I. They are all at least twenty times smaller than the magnitude of the quartic order couplings between the Q_{1x} and Q_{hx} coordinates. Nevertheless, the sign of the coupling coefficients between the Q_{1z} and Q_{hx} modes are such that these terms soften the frequency of the Q_{1z} mode, as one sees by analyzing the forcing terms due to these nonlinear couplings $-\partial V/\partial Q_{1z} = -2lQ_{1z} Q_{hx}^2 - 4m_1 Q_{1z}^3 Q_{hx}^2 - 2m_2 Q_{1z} Q_{hx}^4$. Each term in the previous expression has even powers of the Q_{hx} coordinate, which ensures that their effects are not averaged over the slow oscillation of the

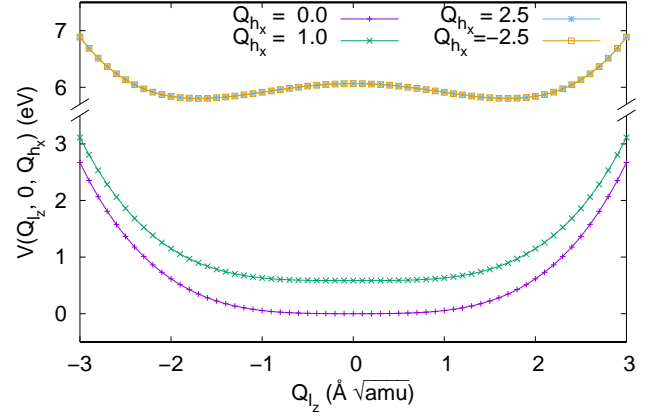


FIG. 3. (Color online) Total energy as a function of the transverse Q_{1z} coordinate for several values of the Q_{hx} coordinate for cubic KTaO₃.

Q_{1z} mode. Furthermore, all these terms are proportional to odd powers of the Q_{1z} coordinate, which causes the frequency of the Q_{1z} mode to change as $\Omega_{1z}^2 \rightarrow \Omega_{1z}^2 [1 + (2lQ_{hx}^2(t) + 4m_1 Q_{1z}^2(t)Q_{hx}^2(t) + 2m_2 Q_{1z}^4(t))/\Omega_{1z}^2]$. Since the coupling constants are negative, this should lead to a softening of the transverse Q_{1z} mode when the Q_{hx} mode is externally pumped.

The above discussion is not sufficient to convincingly argue that the transverse Q_{1z} mode will become dynamically unstable when the Q_{hx} mode is externally pumped. There are two counteracting processes that may preclude this from happening. First, the coupling between the Q_{1x} and Q_{hx} modes is at least twenty times larger. As a result, the Q_{1z} component may receive a much smaller proportion of the external force due to nonlinear coupling with the Q_{hx} mode that is not sufficient to make this mode dynamically unstable when the latter is pumped. Moreover, I find that the coupling term $pQ_{1z}^2 Q_{1x}^2$ to be positive and larger than the term $lQ_{1z}^2 Q_{hx}^2$ (see Table II in the Appendix). When the Q_{1x} component oscillates with a large amplitude, this will provide an additive factor that increases the frequency of the Q_{1z} component.

To settle this issue, I numerically solved the coupled equations of motion of the three coordinates Q_{1z} , Q_{1x} , and Q_{hx} , which are

$$\begin{aligned}
 \ddot{Q}_{hx} + \gamma_h \dot{Q}_{hx} + \Omega_h^2 Q_{hx} &= -\frac{\partial V^{\text{nh}}(Q_{1z}, Q_{1x}, Q_{hx})}{\partial Q_{hx}} + F(t) \\
 \ddot{Q}_{1x} + \gamma_l \dot{Q}_{1x} + \Omega_l^2 Q_{1x} &= -\frac{\partial V^{\text{nh}}(Q_{1z}, Q_{1x}, Q_{hx})}{\partial Q_{1x}} \\
 \ddot{Q}_{1z} + \gamma_l \dot{Q}_{1z} + \Omega_l^2 Q_{1z} &= -\frac{\partial V^{\text{nh}}(Q_{1z}, Q_{1x}, Q_{hx})}{\partial Q_{1z}}. \quad (1)
 \end{aligned}$$

Here, $V^{\text{nh}}(Q_{1z}, Q_{1x}, Q_{hx})$ is the nonharmonic part of the polynomial that fits the calculated energy surface, and it includes both the anharmonicities of each coordinates as well as the nonlinear couplings between these coor-

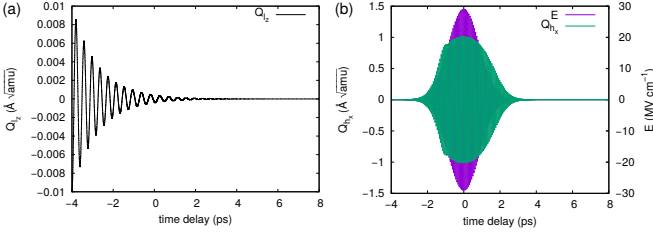


FIG. 4. (Color online) Dynamics of the (a) Q_{1z} and (b) Q_{hx} coordinates of cubic KTaO₃ after the Q_{hx} coordinate is pumped by a pump pulse E with FWHM of 2 ps as shown in (b).

ordinates. The full expression for $V^{\text{nh}}(Q_{1z}, Q_{1x}, Q_{hx})$ is given in Eq. A1 in the Appendix. In addition to the numerically large nonlinear couplings discussed above, it includes anharmonicities up to the sixteenth order and nonlinear couplings up to the eighth order. γ_h and γ_l are the damping coefficients of the highest and lowest frequency T_{1u} modes, respectively. They are taken to be ten percent of the respective harmonic terms. $F(t) = Z_{hx}^* E_0 \sin(\Omega t) e^{-t^2/2(\sigma/2\sqrt{2\ln 2})^2}$ is the external force experienced by the Q_{hx} coordinate due to a light pulse of peak electric field E_0 . The calculated mode effective charge of the Q_{hx} mode of cubic KTaO₃ is $Z_{hx}^* = -1.07e \text{ amu}^{-\frac{1}{2}}$. A pump with a frequency of $\Omega = 1.01\Omega_h$ and FWHM of $\sigma = 2.0$ ps has been used. The use of a long pulse width is just to illustrate many oscillation cycles. The physics does not change when I use a pulse duration larger than $1/\Omega_l$.

The result of the numerical integration of Eq. 1 in a highly nonlinear regime is shown in Fig. 4. This was obtained with a large peak electric field of $E_0 = 30 \text{ MV cm}^{-1}$ that caused the pumped Q_{hx} mode to oscillate with a maximum amplitude of $1.1 \text{ Å}\sqrt{\text{amu}}$ [Fig. 4(b)]. In this regime, the Q_{1x} mode oscillates about the equilibrium position with a maximum amplitude of $0.25 \text{ Å}\sqrt{\text{amu}}$ (not shown). The frequency of its transverse counterpart Q_{1z} does soften by around $\sim 5\%$. But relatively little force is imparted to the Q_{1z} component, and its oscillations about the equilibrium position are damped even during the duration of the pump pulse [Fig. 4(a)]. I performed similar calculations for pump fields up to 100 MV cm^{-1} but was not able to find any instances where the Q_{1z} mode becomes dynamically unstable.

These calculations show that a dynamical instability of the lowest frequency infrared mode of cubic KTaO₃ cannot be achieved by a midinfrared excitation of its highest frequency infrared mode. However, this does not allow us to infer that light-induced dynamical instability cannot occur in any cubic paraelectric. Indeed, if I artificially increase the coefficient of the $lQ_{1z}^2 Q_{hx}^2$ term by six times, I am able to obtain a solution where the Q_{1z} coordinate oscillates about a displaced position during the duration of the pump pulse. Such a large coupling between the pumped high-frequency mode and the transverse component of the low-frequency mode may exist in some mate-

rials.

B. Strained KTaO₃

If the coupling between the externally pumped high-frequency T_{1u} mode and the component of the lowest frequency T_{1u} mode longitudinal to the pumped mode could be weakened in cubic KTaO₃, the transverse component of the lowest frequency mode would develop a light-induced dynamical instability. An effective way of achieving this is by raising the frequency of the longitudinal component relative to that of the transverse component. This can be accomplished by applying a biaxial strain on KTaO₃ via an epitaxial growth on an appropriate substrate.

I performed calculations on KTaO₃ with 0.6% compressive biaxial strain. This can be achieved, for example, by growing KTaO₃ on a GdScO₃ substrate. The calculated PBEsol lattice parameters of thus strained KTaO₃ are $a = b = 3.965$ and $c = 4.0 \text{ Å}$. Upon the application of a biaxial strain, the T_{1u} mode of the cubic phase splits into a nondegenerate A_{2u} mode and a doubly degenerate E_u mode. The A_{2u} phonons involve atomic motions along the z axis while the atoms move in the xy plane for the E_u phonons. The calculated values for the lowest frequency A_{2u} and E_u modes are $\Omega_{1z} = 20$ and $\Omega_{1x} = \Omega_{1y} = 122 \text{ cm}^{-1}$, respectively. The highest frequency E_u phonon that should be externally pumped has a frequency of $\Omega_h = 556 \text{ cm}^{-1}$.

To find out whether the lowest frequency A_{2u} mode Q_{1z} of strained KTaO₃ develops a dynamical instability when the x component of the highest frequency E_u mode Q_{hx} is intensely excited by a light source, I again started my investigation by calculating the total energy surface $V(Q_{1z}, Q_{1x}, Q_{hx})$ as a function of the three coordinates using density functional calculations. The nonlinear couplings between the Q_{1z} , Q_{1x} , and Q_{hx} coordinates of strained KTaO₃ have the same symmetry requirements as discussed for the cubic case, and a fit of a general polynomial to the calculated first-principles $V(Q_{1z}, Q_{1x}, Q_{hx})$ shows that same orders of nonlinearities are present in both the cases. As a comparison of the numbers presented in Table I shows (see also Table II in the Appendix), the nonlinear couplings in the two cases do not differ by a large amount. The crucial difference between the two cases is that the frequencies of the Q_{1z} and Q_{1x} coordinates are different in the strained case ($\Omega_{1z} = 20$ and $\Omega_{1x} = 122 \text{ cm}^{-1}$), whereas they are equal in the cubic case ($\Omega_{1z} = \Omega_{1x} = 85 \text{ cm}^{-1}$). This has a profound effect in the dynamics of the Q_{1z} coordinate because the forces experienced by a coordinate due to the nonlinear couplings are weighted by the square of the frequency of the coordinate. We can see that $\frac{1}{20^2} \frac{\partial V}{\partial Q_{1z}}$ is likely to be much larger than $\frac{1}{122^2} \frac{\partial V}{\partial Q_{1x}}$ or $\frac{1}{85^2} \frac{\partial V}{\partial Q_{1x}}$. In simple words, the Q_{1z} coordinate of strained KTaO₃ gets much larger proportion of the force than the Q_{1x} coordinate of cubic KTaO₃ because the frequency of the Q_{1z} mode is much

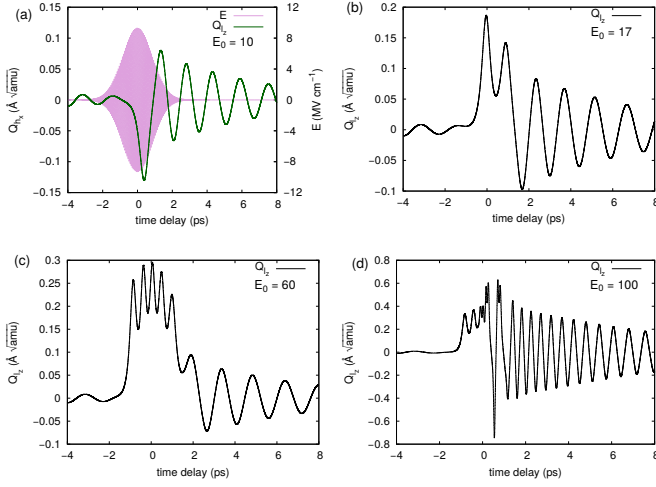


FIG. 5. (Color online) Dynamics of the Q_{1z} coordinate of strained KTaO₃ after the Q_{hx} coordinate is pumped by a pump pulse E with FWHM of 2 ps. The dynamics for four different values of the peak electric field E_0 (MV cm⁻¹) of the pump pulse are shown.

smaller in the strained structure compared to the cubic structure. Is this change big enough to result in a light-induced dynamical instability of the Q_{1z} mode in strained KTaO₃?

I again solved the coupled equations of motion of the three coordinates Q_{hx} , Q_{1x} , and Q_{1z} as given by Eq. 1 for the case of strained KTaO₃. This time I used the potential $V^{nh}(Q_{1z}, Q_{1x}, Q_{hx})$ obtained for strained KTaO₃ from first principles. The polynomial expression used in the calculations and the numerical values of the coefficients for all the terms in the polynomial that fit the calculated energy surface are given in the Appendix. A pump pulse with an FWHM of 2 ps ($> 1/\Omega_{1z}$) and frequency $1.01\Omega_h$ is again used to excite the Q_{hx} mode. The mode effective charge of the Q_{hx} mode in the strained structure is $Z_{hx}^* = -1.15e \text{ amu}^{-\frac{1}{2}}$.

Fig. 5 shows the results of the numerical integration of these equations for three different regimes of dynamics of the Q_{1z} coordinate. At relatively small peak electric fields of the pump ($E_0 < 1 \text{ MV cm}^{-1}$), the Q_{1z} mode oscillates about the equilibrium position with its harmonic frequency (not shown). As the peak electric field is increased, the frequency of the Q_{1z} mode decreases during the duration that the Q_{hx} mode is being pumped [Fig. 5(a)]. As discussed above, this is due to the negative values of the coefficients of the coupling terms $lQ_{1z}^2 Q_{hx}^2$, $m_1 Q_{1z}^4 Q_{hx}^2$, and $m_2 Q_{1z}^2 Q_{hx}^4$ that cause a light-induced softening of the Q_{1z} coordinate. Since the duration of the pump pulse is finite, I naturally do not observe the period of the Q_{1z} mode diverge. Instead, beyond a critical value of the peak electric field of the pump ($E_0^c \simeq 17 \text{ MV cm}^{-1}$ for $\sigma = 2 \text{ ps}$), the Q_{1z} coordinate oscillates about a displaced position and has a non-zero value while the Q_{hx} mode is being pumped [Figs. 5(b, c)]. In this rectified regime, the average potential felt by the Q_{hx} mode

has a double-well structure, and this mode is oscillating about one of the minima. The displacement along the Q_{1z} coordinate is also amplified strongly in this regime. Since the Q_{1z} mode is infrared active, this implies that the material is in a broken symmetry state with a finite dipole moment while the Q_{hx} mode is externally pumped.

The frequency of the Q_{1z} oscillations in the rectified state increases as the peak electric field of the pump is increased beyond the critical threshold. This is evident from a comparison of Figs. 5(b) and (c), which shows that the frequency of the Q_{1z} mode doubles as the peak electric field E_0 is increased from 17 to 60 MV cm⁻¹. This increase occurs because the double-well potential for the Q_{1z} coordinate becomes deeper as the amplitude of the Q_{hx} oscillations increases.

When the peak electric field is increased further ($E_0 > 75 \text{ MV cm}^{-1}$), the Q_{1z} mode oscillates with a large amplitude and high frequency about the equilibrium position [Fig. 5(d)]. In this regime, the kinetic energy imparted to the Q_{1z} mode is larger than the depth of the double wells. As a result, the oscillation of the Q_{1z} mode stops being confined to one of the double wells, and the rectified behavior along the Q_{1z} coordinate is no longer observed. Even though the light-induced broken-symmetry phase is stabilized only for a range of values of the peak electric field of the pump, this range $17 < E_0 < 75 \text{ MV cm}^{-1}$ is both wide and approachable enough to make the light-induced ferroelectric state experimentally accessible.

The existence of a critical threshold above which the Q_{1z} coordinate is rectified and the presence of three different regimes for the dynamics of this coordinate is consistent with the analysis of a $Q_1^2 Q_2^2$ nonlinear coupling between two different normal mode coordinates as presented in Ref. 19. These features should be present in the experiments to confirm the predictions made in this work. The critical pump amplitude depends on the frequencies of the Q_{1z} and Q_{hx} modes and the coupling coefficient, as well as the pump pulse length and the initial condition (i.e. the r.m.s. displacement of the Q_{1z} mode at a particular temperature).¹⁹ For a pump pulse with FWHM of 2 ps, I find that the Q_{1z} mode starts to get rectified when the peak electric field is $E_0 = 17 \text{ MV cm}^{-1}$. With this pump pulse, the Q_{hx} mode is oscillating with an amplitude of $0.9 \text{ Å}\sqrt{\text{amu}}$, which corresponds to a maximum change in the Ta-apical O bond length of 0.2 Å (that is, 10%). The Q_{hx} mode oscillates with an amplitude of $1.3 \text{ Å}\sqrt{\text{amu}}$ when the peak electric field is $E_0 = 75 \text{ MV cm}^{-1}$. This is a modest increase in the energy of the Q_{hx} mode due to the pump, and it indicates that a significant fraction of the pumped energy goes to maintaining the rectified state along the Q_{1z} coordinate. However, the light-induced ferroelectric displacement along the Q_{1z} coordinate is quite small because of the small magnitude of the couplings between Q_{1z} and Q_{hx} modes. The average displacement along Q_{1z} is ~ 0.1 and $\sim 0.2 \text{ Å}\sqrt{\text{amu}}$ for $E_0 = 17$ and 75 MV cm^{-1} , respectively, which results in the change of Ta-apical O distance by $0.015\text{--}0.030 \text{ Å}$.

Curiously, the critical pump threshold obtained for

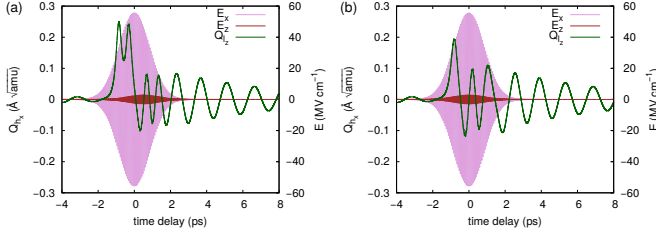


FIG. 6. (Color online) Dynamics of the Q_{1z} coordinate of strained KTaO₃ for the delays of (a) 0.5 and (b) 0.0 ps between the E_{hx} and E_{hz} pulses that pump Q_{hx} and Q_{hz} modes, respectively.

strained KTaO₃ is noticeably smaller than what is expected for a $Q_{1z}^2 Q_{hx}^2$ coupling. In the total energy calculations, the Q_{1z} mode starts developing instability when Q_{hx} is above $0.7 \text{ \AA}\sqrt{\text{amu}}$. So the critical Q_{hx} amplitude should be $0.7\sqrt{2} = 1.0 \text{ \AA}\sqrt{\text{amu}}$.¹⁹ Instead, I find that the Q_{1z} mode becomes unstable when the Q_{hx} amplitude is $0.9 \text{ \AA}\sqrt{\text{amu}}$. This reduction in the critical threshold is due to the presence of a large and negative sixth order coupling terms $m_1 Q_{1z}^4 Q_{hx}^2$ and $m_2 Q_{1z}^2 Q_{hx}^4$. Both these terms give a subtractive contribution to the effective, light-induced frequency of the Q_{1z} mode, which hastens its instability as a function of the pump intensity.

C. Abruptly halting light-induced ferroelectricity

For light-induced ferroelectricity to be useful in applications, it is necessary to be able to control the light-induced phase at will in an all-optical setup. In this context, this means having the capability to switch off the rectification of the Q_{1z} mode while the Q_{hx} mode is being pumped. The quartic order odd $Q_{1z}^3 Q_{hz}$ and $Q_{1z} Q_{hz}^3$ couplings in the longitudinal direction can be used to our advantage for this purpose. To investigate this possibility, I consider an experiment where an overlapping pulse polarized along Q_{hz} comes at an arbitrary delay with respect to the rectification-causing pulse that pumps the Q_{hx} mode. I study the resulting dynamics along the Q_{1z} coordinate by solving the coupled equations of motion for the four coordinates (Q_{1z} , Q_{1x} , Q_{hx} , and Q_{hz}). The equations of motions are obtained from the potential $V^{\text{nh}}(Q_{1z}, Q_{1x}, Q_{hx}) + V^{\text{nh}}(Q_{1z}, Q_{hz})$. For computational efficiency, I do not consider the full potential $V^{\text{nh}}(Q_{1z}, Q_{1x}, Q_{hx}, Q_{hz})$ spanned by the four coordinates.

The results for the delays of 0.5 and 0.0 ps between the pump pulses E_{hx} and E_{hz} that excite the Q_{hx} and Q_{hz} coordinates, respectively, are shown in Fig. 6. The peak electric fields of E_{hx} and E_{hz} are 60 and 3 MV cm⁻¹, respectively, and their FWHM is 2 ps. The pump frequencies are 1.01 times the respective phonon frequencies and the mode effective charge of Q_{hz} is $Z_{hz}^* = -1.05e \text{ amu}^{-\frac{1}{2}}$. Note that excitation by only E_{hx} causes rectification of the Q_{1z} mode during the FWHM of the pulse

[Fig. 5(c)]. However, an overlapping excitation by another weak pulse E_{hz} immediately suppresses the light-induced rectification of the Q_{1z} mode. Even a weak longitudinal pump is efficient in halting the rectification because the quartic order odd couplings between Q_{1z} and Q_{hz} modes are much larger than the couplings in the transverse direction.

IV. SUMMARY AND CONCLUSIONS

In summary, I have shown that midinfrared pulses can be used to stabilize nonequilibrium ferroelectricity in strained KTaO₃, which is paraelectric at equilibrium conditions. This phenomenon relies on a quartic $l Q_{1z}^2 Q_{hx}^2$ coupling between the highest frequency infrared-active phonon mode Q_{hx} and the lowest frequency infrared-active mode Q_{1z} that is transverse to Q_{hx} . Density functional calculations show that the coupling constant l is negative, which causes the Q_{1z} mode to soften when the Q_{hx} mode is externally pumped. The rectification along the Q_{1z} coordinate occurs only above a critical electric field of the pump pulse, demonstrating that this light-induced symmetry breaking is a unique nonperturbative effect. Such a threshold behavior should be observed in experiments to corroborate the predictions made in this paper. Additionally, the $Q_{1z}^4 Q_{hx}^2$ and $Q_{1z}^2 Q_{hx}^4$ couplings are large, and this makes the rectified regime more accessible. A first principles calculation of the coupling between light and the Q_{hx} mode shows that ferroelectricity can be induced in strained KTaO₃ by a midinfrared pulse with a peak electric field of 17 MV cm⁻¹ and a duration of 2 ps. Furthermore, large odd quartic couplings $Q_{1z}^3 Q_{hz}$ and $Q_{1z} Q_{hz}^3$ between Q_{1z} and the highest frequency infrared-active mode Q_{hz} longitudinal to Q_{1z} makes it possible to arbitrarily switch off the induced ferroelectricity by pumping the Q_{hz} mode with another weak pulse. I find that similar nonlinear interactions exist in SrTiO₃ and LaAlO₃, and this technique could be generally applied to other transition metal oxide paraelectrics.

At a more basic level, I have shown that materials can exhibit various nonlinear interactions between different dynamical degrees of freedom that have hitherto been overlooked. These interactions enable us to induce and control broken-symmetry phases using light, whose oscillating electric and magnetic fields average to zero by definition. Furthermore, I have demonstrated that the nonlinear interactions can be effectively modified by applying strain. This motivates experiments that combine the disparate fields of nonlinear optics and heterostructuring to achieve materials control in an interesting manner. In a broader perspective, these nonlinear interactions may also be present in other classes of systems, and they might allow us to influence the dynamics of these systems in an unusual way.

ACKNOWLEDGMENTS

I am grateful to Indranil Paul for helpful discussions. This work was supported by the European Research Council grants ERC-319286 QMAC and ERC-61719 CORRELMAT and the Swiss National Supercomputing Center (CSCS) under project s575.

Appendix A: Expressions for total energy surfaces

Only low order nonlinear couplings that are relatively large were discussed in the main text. However, if only low order couplings and anharmonicities are considered, the fit to the calculated total-energy surfaces are not satisfactory. The dynamics of the coordinates with and without using the high order couplings also show large differences, especially at the nonlinear regime. Since the use of the full polynomial expression in the solutions of the equations of motion are not computationally demanding, all the numerical results discussed in this paper were obtained using the full expression given below.

For cubic KTaO₃, the following polynomial $V(Q_{1z}, Q_{1x}, Q_{hx})$ accurately fits the calculated total energy surface spanned by the three coordinates for values between -3.0 and $3.0 \text{ \AA}\sqrt{\text{amu}}$.

$$\begin{aligned}
 V = & \frac{1}{2}\Omega_{1z}^2 Q_{1z}^2 + a_4 Q_{1z}^4 + a_6 Q_{1z}^6 + a_8 Q_{1z}^8 + a_{10} Q_{1z}^{10} \\
 & + a_{12} Q_{1z}^{12} + a_{14} Q_{1z}^{14} + a_{16} Q_{1z}^{16} + \frac{1}{2}\Omega_{1x}^2 Q_{1x}^2 + a_4 Q_{1x}^4 \\
 & + a_6 Q_{1x}^6 + a_8 Q_{1x}^8 + a_{10} Q_{1x}^{10} + a_{12} Q_{1x}^{12} + a_{14} Q_{1x}^{14} \\
 & + a_{16} Q_{1x}^{16} + \frac{1}{2}\Omega_{hx}^2 Q_{hx}^2 + c_4 Q_{hx}^4 + c_6 Q_{hx}^6 + c_8 Q_{hx}^8 \\
 & + c_{10} Q_{hx}^{10} + c_{12} Q_{hx}^{12} + l Q_{1z}^2 Q_{hx}^2 + m_1 Q_{1z}^4 Q_{hx}^2 \\
 & + m_2 Q_{1z}^2 Q_{hx}^4 + n_1 Q_{1z}^4 Q_{hx}^4 + n_2 Q_{1z}^6 Q_{hx}^2 + n_3 Q_{1z}^2 Q_{hx}^6 \\
 & + t_1 Q_{1x}^3 Q_{hx} + t_2 Q_{1x}^2 Q_{hx}^2 + t_3 Q_{1x} Q_{hx}^3 + u_1 Q_{1x}^5 Q_{hx} \\
 & + u_2 Q_{1x}^4 Q_{hx}^2 + u_3 Q_{1x}^3 Q_{hx}^3 + u_4 Q_{1x}^2 Q_{hx}^4 + u_5 Q_{1x} Q_{hx}^5 \\
 & + p Q_{1z}^2 Q_{1x}^2 + q_1 Q_{1z}^4 Q_{1x}^2 + q_2 Q_{1z}^2 Q_{1x}^4 + r_1 Q_{1z}^4 Q_{1x}^4 \\
 & + r_2 Q_{1z}^6 Q_{1x}^2 + r_3 Q_{1z}^2 Q_{1x}^6 + d Q_{1z}^2 Q_{1x} Q_{hx} \\
 & + e_1 Q_{1z}^2 Q_{1x}^3 Q_{hx} + e_2 Q_{1z}^2 Q_{1x}^2 Q_{hx}^2 + e_3 Q_{1z}^2 Q_{1x} Q_{hx}^3 \\
 & + f_1 Q_{1z}^2 Q_{1x}^5 Q_{hx} + f_2 Q_{1z}^2 Q_{1x}^4 Q_{hx}^2 + f_3 Q_{1z}^2 Q_{1x}^3 Q_{hx}^3 \\
 & + f_4 Q_{1z}^2 Q_{1x}^2 Q_{hx}^4 + f_5 Q_{1z}^2 Q_{1x} Q_{hx}^5 + g Q_{1z}^4 Q_{1x} Q_{hx} \\
 & + h_1 Q_{1z}^4 Q_{1x}^3 Q_{hx} + h_2 Q_{1z}^4 Q_{1x}^2 Q_{hx}^2 + h_3 Q_{1z}^4 Q_{1x} Q_{hx}^3.
 \end{aligned} \tag{A1}$$

For strained KTaO₃, the potential has additional $a_{18} Q_{1z}^{18}$ and $a_{20} Q_{1z}^{20}$ terms. Also, the coefficients of the Q_{1z}^n and Q_{1x}^n terms are different in the strained case. The coefficients of the Q_{1x}^n terms for the strained case are denoted by b_n in Table II.

The polynomial $V(Q_{1z}, Q_{hx})$ that fits the energy surface spanned by the Q_{1z} and Q_{hx} coordinates is given

by

$$\begin{aligned}
 V = & \frac{1}{2}\Omega_{1z}^2 Q_{1z}^2 + a_4 Q_{1z}^4 + a_6 Q_{1z}^6 + a_8 Q_{1z}^8 + a_{10} Q_{1z}^{10} \\
 & + a_{12} Q_{1z}^{12} + a_{14} Q_{1z}^{14} + a_{16} Q_{1z}^{16} + a_{18} Q_{1z}^{18} + a_{20} Q_{1z}^{20} \\
 & + \frac{1}{2}\Omega_{hx}^2 Q_{hx}^2 + d_4 Q_{hx}^4 + d_6 Q_{hx}^6 + d_8 Q_{hx}^8 + d_{10} Q_{hx}^{10} \\
 & + d_{12} Q_{hx}^{12} + v_1 Q_{1z}^3 Q_{hx} + v_2 Q_{1z}^2 Q_{hx}^2 + v_3 Q_{1z} Q_{hx}^3 \\
 & + w_1 Q_{1z}^5 Q_{hx} + w_2 Q_{1z}^4 Q_{hx}^2 + w_3 Q_{1z}^3 Q_{hx}^3 + w_4 Q_{1z}^2 Q_{hx}^4 \\
 & + w_5 Q_{1z} Q_{hx}^5.
 \end{aligned} \tag{A2}$$

The nonharmonic potential V^{nh} defined in the main text is V without the harmonic $\frac{1}{2}\Omega Q^2$ terms. The values of all the coefficients in Eqs. A1 and A2 obtained from a fit to the calculated energy surfaces of cubic and strained KTaO₃ are given in Table II. I note that values lower than the magnitude of 10^{-5} are below the accuracy of the density functional calculations. They are kept so that that the highest order anharmonicity has a positive sign, which keeps the numerical solution of the equation of motions stable.

Appendix B: Mode effective charges

The mode effective charge vector $Z_{m,\alpha}^* = \partial F_{m,\alpha} / \partial E_\alpha$ relates the force $F_{m,\alpha}$ experienced by the normal mode coordinate Q_m due to an electric field E_α along the direction α . It is related to the Born effective charges $Z_{\kappa,\alpha\beta}^*$ of atoms κ in the unit cell of a material by³¹

$$Z_{m,\alpha}^* = \sum_{\kappa,\beta} Z_{\kappa,\alpha\beta}^* U_m(\kappa, \beta),$$

where $U_m(\kappa, \beta)$ is the $\mathbf{q} = 0$ eigendisplacement vector normalized as

$$\sum_{\kappa,\beta} M_\kappa [U_m(\kappa, \beta)]^* U_n(\kappa, \beta) = \delta_{mn}.$$

Here M_κ is the mass of the atom κ . The eigendisplacement vector is related to the eigenvector $w_m(\kappa, \beta)$ of the dynamical matrix by

$$U_m(\kappa, \beta) = \frac{w_m(\kappa, \beta)}{\sqrt{M_\kappa}}.$$

Note that this definition of the mode effective charge is slightly different from the one used in Ref. 31. Here, $Z_{m,\alpha}^*$ is related to the change in the value of the normal mode coordinate rather than the change in the atomic displacements due to a motion along the normal mode coordinate. This gives a different normalization factor for $Z_{m,\alpha}^*$, and this quantity is expressed in the units of $e \text{ amu}^{-\frac{1}{2}}$. Its sign is arbitrary because the eigenvector of the dynamical matrix is defined up to a multiplicative constant.

TABLE II. The coefficients of the harmonic, anharmonic and nonlinear coupling terms of cubic and strained KTaO_3 . The units of a $Q^m Q^n Q^p$ term are $\text{meV } \text{\AA}^{-(m+n+p)} \text{ amu}^{\frac{-(m+n+p)}{2}}$. The sign of the coupling is relevant only when the coordinates come with even powers.

coefficient	order	cubic	strained	coefficient	order	strained
Ω_{1z}^2	Q_{1z}^2	27.06	1.39	Ω_{hz}^2	Q_{hz}^2	1034.38
Ω_{1x}^2	Q_{1x}^2	27.06	55.27	b_4	Q_{1x}^4	36.56
Ω_h^2	Q_{hx}^2	1043.77	1136.10	b_6	Q_{1x}^{6x}	-5.05
a_4	Q_{1z}^4	47.55	51.72	b_8	Q_{1x}^{8x}	1.12
a_6	Q_{1z}^6	-6.45	-8.69	b_{10}	Q_{1x}^{10}	-1.79×10^{-1}
a_8	Q_{1z}^8	1.47	2.73	b_{12}	Q_{1x}^{12}	1.85×10^{-2}
a_{10}	Q_{1z}^{10}	-2.35×10^{-1}	-6.91×10^{-1}	b_{14}	Q_{1x}^{14}	-1.07×10^{-3}
a_{12}	Q_{1z}^{12}	2.43×10^{-2}	1.28×10^{-1}	b_{16}	Q_{1x}^{16}	2.64×10^{-5}
a_{14}	Q_{1z}^{14}	-1.41×10^{-3}	-1.61×10^{-2}	d_4	Q_{hz}^4	61.23
a_{16}	Q_{1z}^{16}	3.47×10^{-5}	1.30×10^{-3}	d_6	Q_{hz}^6	-7.24×10^{-1}
a_{18}	Q_{1z}^{18}		-6.04×10^{-5}	d_8	Q_{hz}^8	3.97×10^{-1}
a_{20}	Q_{1z}^{20}		1.23×10^{-6}	d_{10}	Q_{hz}^{10}	-1.38×10^{-2}
c_4	Q_{hx}^4	63.17	78.60	d_{12}	Q_{hz}^{12}	5.99×10^{-5}
c_6	Q_{hx}^6	-7.33×10^{-1}	-1.00	v_1	$Q_{1z}^3 Q_{hz}$	119.42
c_8	Q_{hx}^8	4.38×10^{-1}	7.22	v_2	$Q_{1z}^2 Q_{hz}^2$	212.45
c_{10}	Q_{hx}^{10}	-1.68×10^{-2}	-3.79×10^{-2}	v_3	$Q_{1z} Q_{hz}^3$	169.37
c_{12}	Q_{hx}^{12}	1.29×10^{-4}	6.49×10^{-4}	w_1	$Q_{1z}^5 Q_{hz}$	2.88
l	$Q_{1z}^2 Q_{hx}^2$	-5.95	-5.81	w_2	$Q_{1z}^4 Q_{hz}^2$	11.23
m_1	$Q_{1z}^4 Q_{hx}^2$	-1.03	-1.00	w_3	$Q_{1z}^3 Q_{hz}^3$	23.54
m_2	$Q_{1z}^2 Q_{hx}^4$	-3.05	-4.12	w_4	$Q_{1z}^2 Q_{hz}^4$	25.42
n_1	$Q_{1z}^4 Q_{hx}^4$	1.85×10^{-1}	2.41×10^{-1}	w_5	$Q_{1z} Q_{hz}^5$	13.46
n_2	$Q_{1z}^6 Q_{hx}^2$	4.35×10^{-3}	0.00			
n_3	$Q_{1z}^2 Q_{hx}^6$	-2.37×10^{-1}	-3.14×10^{-1}			
t_1	$Q_{1x}^3 Q_{hx}$	-118.35	97.38			
t_2	$Q_{1x}^2 Q_{hx}^2$	215.00	208.76			
t_3	$Q_{1x} Q_{hx}^3$	-175.58	195.22			
u_1	$Q_{1x}^5 Q_{hx}$	-2.72	1.73			
u_2	$Q_{1x}^4 Q_{hx}^2$	10.64	6.93			
u_3	$Q_{1x}^3 Q_{hx}^3$	-22.81	18.34			
u_4	$Q_{1x}^2 Q_{hx}^4$	25.38	24.27			
u_5	$Q_{1x} Q_{hx}^5$	-13.70	15.57			
p	$Q_{1z}^2 Q_{1x}^2$	6.29	6.02			
q_1	$Q_{1z}^4 Q_{1x}^2$	-1.70	-1.56			
q_2	$Q_{1z}^2 Q_{1x}^4$	-1.70	-1.39			
r_1	$Q_{1z}^4 Q_{1x}^4$	9.35×10^{-2}	7.39×10^{-2}			
r_2	$Q_{1z}^6 Q_{1x}^2$	5.23×10^{-3}	7.12×10^{-3}			
r_3	$Q_{1z}^2 Q_{1x}^6$	5.23×10^{-3}	1.45×10^{-2}			
d	$Q_{1z}^2 Q_{1x} Q_{hx}$	-19.09	15.02			
e_1	$Q_{1z}^2 Q_{1x}^3 Q_{hx}$	6.61	-5.5			
e_2	$Q_{1z}^2 Q_{1x}^2 Q_{hx}^2$	-13.16	-13.62			
e_3	$Q_{1z}^2 Q_{1x} Q_{hx}^3$	11.32	-13.03			
f_1	$Q_{1z}^2 Q_{1x}^5 Q_{hx}$	2.99×10^{-1}	-2.06×10^{-1}			
f_2	$Q_{1z}^2 Q_{1x}^4 Q_{hx}^2$	-6.80×10^{-1}	-4.44×10^{-1}			
f_3	$Q_{1z}^2 Q_{1x}^3 Q_{hx}^3$	1.39	-1.10			
f_4	$Q_{1z}^2 Q_{1x}^2 Q_{hx}^4$	-1.45	-1.34			
f_5	$Q_{1z}^2 Q_{1x} Q_{hx}^5$	8.75×10^{-1}	-9.52×10^{-1}			
g	$Q_{1z}^4 Q_{1x} Q_{hx}$	1.02	-4.06×10^{-1}			
h_1	$Q_{1z}^4 Q_{1x}^3 Q_{hx}$	-4.62×10^{-1}	3.31×10^{-1}			
h_2	$Q_{1z}^4 Q_{1x}^2 Q_{hx}^2$	8.13×10^{-1}	7.51×10^{-1}			
h_3	$Q_{1z}^4 Q_{1x} Q_{hx}^3$	-7.45×10^{-1}	7.51×10^{-1}			

The mode effective charge can be experimentally determined. It is related to the ionic contribution to the dielectric constant by³¹

$$\epsilon_{\alpha\beta}(\Omega) = \epsilon_{\alpha\beta}^{\infty} + \frac{4\pi}{V_0} \sum_m \frac{Z_{m,\alpha}^* Z_{m,\beta}^*}{\Omega_m^2 - \Omega^2},$$

where V_0 is the unit cell volume and Ω_m is the frequency of the mode m . This expression shows that the oscillator strength measured in optical spectroscopy is the square of the mode effective charge.

-
- ¹ A. Suzuki and T. Tanaka, *Nature* **346**, 345 (1990).
 - ² S. Koshihara, Y. Tokura, T. Mitani, G. Saito, and T. Koda, *Phys. Rev. B* **42**, 6853(R) (1990).
 - ³ S. Decurtins, P. Gutlich, C. P. Kohler, H. Spiering, and A. Hauser, *Chem. Phys. Lett.* **105**, 1 (1984).
 - ⁴ K. Miyano, T. Tanaka, Y. Tomioka, and Y. Tokura, *Phys. Rev. Lett.* **78**, 4257 (1997).
 - ⁵ L. Stojchevska, I. Vaskivskyi, T. Mertelj, P. Kusar, D. Svetin, S. Brazovskii, and D. Mihailovic, *Science* **344**, 177 (2014).
 - ⁶ M. Rini, R. Tobey, N. Dean, J. Itatani, Y. Tomioka, Y. Tokura, R. W. Schoenlein, and A. Cavalleri, *Nature* **449**, 72 (2007).
 - ⁷ A. D. Caviglia, R. Scherwitzl, P. Popovich, W. Hu, H. Bromberger, R. Singla, M. Mitrano, M. C. Hoffmann, S. Kaiser, P. Zubko *et al.*, *Phys. Rev. Lett.* **108**, 136801 (2012).
 - ⁸ R. I. Tobey, D. Prabhakaran, A. T. Boothroyd, and A. Cavalleri, *Phys. Rev. Lett.* **101**, 197404 (2008).
 - ⁹ M. Först, R. I. Tobey, S. Wall, H. Bromberger, V. Khanna, A. L. Cavalleri, Y.-D. Chuang, W. S. Lee, R. Moore, W. F. Schlotter *et al.*, *Phys. Rev. B* **84**, 241104(R) (2011).
 - ¹⁰ M. Först, A. D. Caviglia, R. Scherwitzl, R. Mankowsky, P. Zubko, V. Khanna, H. Bromberger, S. B. Wilkins, Y.-D. Chuang, W. S. Lee *et al.* *Nat. Mater.* **14**, 883 (2015).
 - ¹¹ D. Fausti, R. I. Tobey, N. Dean, S. Kaiser, A. Dienst, M. C. Hoffmann, S. Pyon, T. Takayama, H. Takagi, and A. Cavalleri, *Science* **331**, 189 (2011).
 - ¹² S. Kaiser, C. R. Hunt, D. Nicoletti, W. Hu, I. Gierz, H. Y. Liu, M. Le Tacon, T. Loew, D. Haug, B. Keimer, and A. Cavalleri, *Phys. Rev. B* **89**, 184516 (2014).
 - ¹³ W. Hu, S. Kaiser, D. Nicoletti, C. R. Hunt, I. Gierz, M. C. Hoffmann, M. Le Tacon, T. Loew, B. Keimer, and A. Cavalleri, *Nat. Mater.* **13**, 705 (2014).
 - ¹⁴ M. Mitrano, A. Cantaluppi, D. Nicoletti, S. Kaiser, A. Perucchi, S. Lupi, P. Di Pietro, D. Pontiroli, M. Ricc, S. R. Clark, D. Jaksch, and A. Cavalleri, *Nature* **530**, 461 (2016).
 - ¹⁵ J. T. Kindt and C. A. Schmuttenmaer, *J. Chem. Phys.* **110**, 8589 (1999).
 - ¹⁶ J. Orenstein and J. S. Dodge, *Phys. Rev. B* **92**, 134507 (2015).
 - ¹⁷ M. Först, C. Manzoni, S. Kaiser, Y. Tomioka, Y. Tokura, R. Merlin, and A. Cavalleri, *Nat. Phys.* **7**, 854 (2011).
 - ¹⁸ M. Först, R. Mankowsky, H. Bromberger, D. M. Fritz, H. Lemke, D. Zhu, M. Chollet, Y. Tomioka, Y. Tokura, R. Merlin, J. P. Hill, S. L. Johnson, and A. Cavalleri, *Solid State Commun.* **169**, 24 (2013).
 - ¹⁹ A. Subedi, A. Cavalleri, and A. Georges, *Phys. Rev. B* **89**, 220301(R) (2014).
 - ²⁰ R. Mankowsky, A. Subedi, M. Först, S. O. Mariager, M. Chollet, H. T. Lemke, J. S. Robinson, J. M. Glowia, M. P. Minitti, A. Frano *et al.*, *Nature* **516**, 71 (2014).
 - ²¹ R. F. Wallis and A. A. Maradudin, *Phys. Rev. B* **3**, 2063 (1971).
 - ²² T. P. Martin and L. Genzel, *Phys. Status Solidi B* **61**, 493 (1974).
 - ²³ M. Fechner and N. A. Spaldin, *Phys. Rev. B* **94**, 134307 (2016).
 - ²⁴ D. M. Juraschek, M. Fechner, and N. A. Spaldin, *cond-mat*, arXiv:1607.01653 (2016).
 - ²⁵ Ref. 24 claims that a $Q_R Q_{IR_1} Q_{IR_2}$ (with $1 \neq 2$) coupling causes a rectification along Q_R . However, such a coupling actually leads to an oscillation of the Q_R mode with an envelop frequency $\Omega_{IR_1} - \Omega_{IR_2}$.
 - ²⁶ A. Subedi, *Phys. Rev. B* **92**, 214303 (2015).
 - ²⁷ J. P. Perdew, A. Ruzsinszky, G. I. Csonka, O. A. Vydrov, G. E. Scuseria, L. A. Constantin, X. Zhou, and K. Burke, *Phys. Rev. Lett.* **100**, 136406 (2008).
 - ²⁸ K. Parlinski, Z.-Q. Li, and Y. Kawazoe, *Phys. Rev. Lett.* **78**, 4063 (1997).
 - ²⁹ A. Togo, F. Oba, and I. Tanaka, *Phys. Rev. B* **78**, 134106 (2008).
 - ³⁰ S. Baroni, S. de Gironcoli, A. Dal Corso, and P. Giannozzi, *Rev. Mod. Phys.* **73**, 515 (2001).
 - ³¹ X. Gonze and C. Lee, *Phys. Rev. B* **55**, 10355 (1997).
 - ³² J. W. Eaton, D. Bateman, S. Hauberg, and R. Wehbring, *GNU Octave version 4.0.0 manual: a high-level interactive language for numerical computations* <http://www.gnu.org/software/octave/doc/interpreter> (2015).
 - ³³ K. Takahashi, N. Kida, and M. Tonouchi, *Phys. Rev. Lett.* **96**, 117402 (2006).
 - ³⁴ D. Talbayev, S. Lee, S.-W. Cheong, and A. J. Taylor, *Appl. Phys. Lett.* **93**, 212906 (2008).
 - ³⁵ J. F. Scott, *Rev. Mod. Phys.* **46**, 83 (1974).
 - ³⁶ D. J. Singh, *Phys. Rev. B* **53**, 176 (1996).
 - ³⁷ H. Vogt and H. Uwe, *Phys. Rev. B* **29**, 1030 (1984).